

Title	Structure and Raman scattering of Cs ₃ C₆₀ under high pressure
Author(s)	Fujiki, S.; Kubozono, Y.; Emura, S.; Takabayashi, Y.; Kashino, S.; Fujiwara, A.; Ishii, K.; Suematsu, H.; Murakami, Y.; Iwasa, Y.; Mitani, T.; Ogata, H.
Citation	Physical Review B, 62(9): 5366-5369
Issue Date	2000-09-01
Type	Journal Article
Text version	publisher
URL	http://hdl.handle.net/10119/4601
Rights	S. Fujiki, Y. Kubozono, S. Emura, Y. Takabayashi, S. Kashino, A. Fujiwara, K. Ishii, H. Suematsu, Y. Murakami, Y. Iwasa, T. Mitani, and H. Ogata, Physical Review B, 62(9), 2000, 5366-5369. Copyright 2000 by the American Physical Society. http://link.aps.org/abstract/PRB/v62/p5366
Description	

Structure and Raman scattering of Cs_3C_{60} under high pressure

S. Fujiki,¹ Y. Kubozono,^{1,*} S. Emura,² Y. Takabayashi,¹ S. Kashino,¹ A. Fujiwara,³ K. Ishii,³ H. Suematsu,³
Y. Murakami,⁴ Y. Iwasa,⁵ T. Mitani,⁵ and H. Ogata⁶

¹*Department of Chemistry, Okayama University, Okayama 700-8530, Japan*

²*ISIR, Osaka University, Osaka 567-0047, Japan*

³*Department of Physics, University of Tokyo, Tokyo 113-0033, Japan*

⁴*KEK-PF, Tsukuba 305-0801, Japan*

⁵*Japan Advanced Institute of Science and Technology, Ishikawa 923-1292, Japan*

⁶*Institute for Molecular Science, Okazaki 444-8585, Japan*

(Received 4 October 1999; revised manuscript received 24 January 2000)

Raman scattering is studied for a pressure-induced superconductor Cs_3C_{60} in a pressure region from 1 bar to 62 kbar. The center frequency ω_0 for $H_g(1)$ and $H_g(2)$ Raman peaks increase by applying pressure, but the increase shows a saturation in the high-pressure region. On the other hand, the ω_0 for $A_g(1)$ and $A_g(2)$ modes increase monotonically in all pressure regions. The electron-phonon coupling constant for Cs_3C_{60} shows a rapid decrease up to 30 kbar and an increase above 30 kbar. This result may be associated with a transformation from a multiphase (body-centered orthorhombic and *A15* phases) to a single phase around 20 kbar. X-ray powder diffraction pattern at 11 K under a pressure of 40 kbar shows that a superconducting phase for Cs_3C_{60} is body-centered orthorhombic.

In 1995, Palstra *et al.* found that Cs_3C_{60} was a pressure-induced superconductor that exhibited at 14.3 kbar the highest superconducting critical temperature ($T_c = 40$ K) among fullerene superconductors.¹ According to their observation, the T_c appeared by applying pressure and increased with an increase in pressure. This increase in T_c is contrary to the model that a band broadening by applying pressure reduces the density-of-state on the Fermi level, $N(\epsilon_F)$, and T_c as expected from the BCS theory. One of the explanations for the increase is that the shielding currents are suppressed by a disorder such as fine grain and the two-phase nature of body-centered tetragonal (bct) and *A15* at 1 bar.¹ Such a disorder may reduce T_c by a fluctuation in the phase of the superconducting order parameter Ψ . If only one phase is realized under high pressure, applying pressure should lead to a decrease in the fluctuation of Ψ and improve the superconducting phase. The second explanation is that applying pressure can reduce the phase fluctuation of Ψ and increase the T_c because pressing the grains should improve the connectivity of the material. The third explanation is based on the assumption that Cs_3C_{60} is a Mott-Hubbard insulator. The superconducting transition cannot be expected for an insulating Cs_3C_{60} because all known fullerene superconductors transform to a superconducting state from a metallic state. Applying pressure may change an insulating state to a metallic state, and further a superconducting state.

We studied the structure and physical properties of Cs_3C_{60} at 1 bar by x-ray powder diffraction and ESR (electron spin resonance)² and found that Cs_3C_{60} at 1 bar took two phases of body-centered orthorhombic (bco; *Immm*, not bct) as the major phase and *A15* as the minor phase from 10 to 300 K. It was recently found that Cs_4C_{60} also took a bco structure.³ No metal-insulator transition was observed for Cs_3C_{60} by ESR from 1.9 to 300 K at 1 bar,² suggesting that it is not the Mott-Hubbard insulator. The electron-phonon (e-ph) coupling constant λ determined for Cs_3C_{60} from Raman scattering at 1 bar was ~ 0.18 , which was approximately one third of Rb_3C_{60} and K_3C_{60} .⁴ The λ for Cs_3C_{60} estimated from Ra-

man scattering at 1 bar does not lead to any meaningful T_c in the BCS and McMillan theory, which is consistent with non-superconductivity at 1 bar. In the present paper, we studied the Raman scattering of Cs_3C_{60} from 1 bar to 62 kbar with an interest in the e-ph coupling under high pressure for a pressure-induced superconductor. Further, we studied the crystal structures of Cs_3C_{60} at 101 and 11 K under a pressure of 40 kbar, which corresponds to the normal and the superconducting states, respectively.

The sample of Cs_3C_{60} was prepared by using liquid NH_3 at low temperature according to the method reported in Ref. 1. After removing NH_3 by pumping under 10^{-3} Torr at 100 °C for 18 h and at 140 °C for 1 h, the sample was transferred into a capillary (outer diameter $\phi = 0.7$ mm) and a diamond anvil cell in a glove box for Raman and x-ray diffraction measurements. X-ray diffraction pattern at 298 K and 1 bar was measured with $\text{CuK}\alpha$ radiation (wavelength: 1.5418 Å) by an x-ray diffractometer (Rigaku Rint 1500). X-ray powder diffraction patterns were measured at 11 and 101 K under a pressure of 40 kbar with synchrotron radiation (wavelength: 0.6896 Å) at BL-1B of the Photon Factory in the High Energy Accelerator Research Organization. The Rietveld analyses for x-ray diffraction patterns were achieved by using RIETAN 94 program.⁵ The Raman scattering was measured at 298 K with He-Ne laser excitation of 632.8 nm using a Confocal Raman Imaging LabRam system. The center frequency ω_0 , the line width Γ , and the asymmetric parameter q for the Raman peak, were determined by a least-squares fitting with the Breit-Wigner-Fano (BWF) formula. The $H_g(2)$ peaks were analyzed by the three-components fitting, while the $H_g(1)$, $A_g(1)$, and $A_g(2)$ peaks were analyzed by the single-component fitting. The multiple splittings of the $H_g(2)$ mode have been observed in single crystals of K_3C_{60} and Rb_3C_{60} .⁶ The splittings suggest a lowering of symmetry from Ih for the C_{60} molecule, which is reasonable for the Cs_3C_{60} crystal of *Immm*. The $H_g(1)$ and $H_g(2)$ modes showed a large $1/q$ as observed previously,⁴ which reflects the BWF effect. The $A_g(1)$ and $A_g(2)$ peaks showed

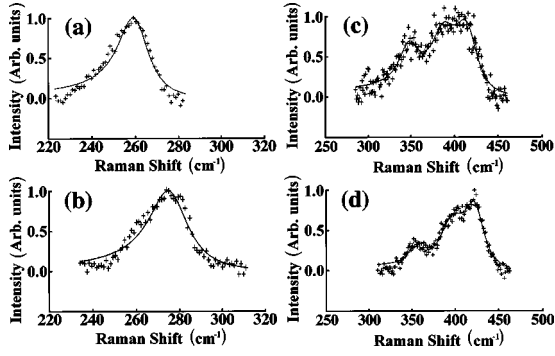


FIG. 1. Raman peaks for the $H_g(1)$ mode at (a) 6 and (b) 47 kbar, and those for the $H_g(2)$ mode at (c) 6 and (d) 47 kbar. The $H_g(1)$ and $H_g(2)$ modes were analyzed by a single BWF and three BWF components, respectively. The crosses and solid lines refer to the experimental and the best-fitted peaks, respectively.

a small $1/q$, i.e., a Lorentzian line shape. The coupling between the phonon and a low-energy continuum ($t_{1u}-t_{1u}^*$ interband transition caused by a lowering in symmetry of the C_{60} molecule) is the origin of the BWF effect in the H_g modes.⁷

The $A_g(2)$ Raman peak was observed at ω_0 of 1447 cm^{-1} at 1 bar. The ω_0 value was consistent with those reported previously.^{1,2,4} Further, the ω_0 for the $H_g(1)$ (259 cm^{-1}) and $A_g(1)$ (493 cm^{-1}) modes were consistent with those reported previously.⁴ The ω_0 for the $H_g(4)$ peak was 756 cm^{-1} , which was close to that in K_3C_{60} .⁶ The x-ray diffraction pattern at 1 bar was also consistent with that reported previously,^{1,2,4} and the Rietveld analysis showed the occupancy of 0.75 for Cs atom. These results support that this sample is Cs_3C_{60} .

As a typical example of the Raman scattering in the present study, the $H_g(1)$, $H_g(2)$, $A_g(1)$, and $A_g(2)$ Raman peaks observed at 6 and 47 kbar are shown in Figs. 1 and 2 along with the calculated Raman peaks, in order to show the quality of the Raman data and the validity of the analyses. The Raman data and the analyses in all pressure regions were sufficient to estimate the pressure dependence of the e-ph coupling in Cs_3C_{60} . The values of ω_0 and Γ for the Raman peaks at 1 bar, 6 kbar, and 47 kbar are collected in Table I.

Figures 3(a) and 3(b) show the pressure dependence of the ω_0 and Γ for the $H_g(1)$ peak. The ω_0 increases with an

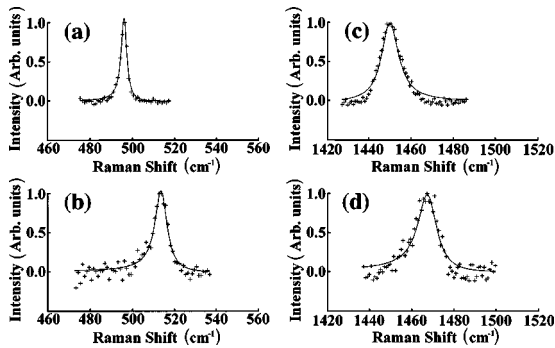


FIG. 2. Raman peaks for the $A_g(1)$ mode at (a) 6 and (b) 47 kbar, and those for the $A_g(2)$ mode at (c) 6 and (d) 47 kbar. Both modes were analyzed by a single BWF component, respectively. The crosses and solid lines refer to the experimental and the best-fitted peaks, respectively.

TABLE I. Values of ω_0 (cm^{-1}) and Γ (cm^{-1}) for the Raman modes at 1 bar, 6 kbar, and 47 kbar.

Mode	P	ω_0	Γ	ω_0	Γ	ω_0	Γ	$\langle\omega_0\rangle^a$	$\langle\Gamma\rangle^a$
$H_g(1)$	1 bar	259	8						
	6 kbar	260	9						
	47 kbar	277	11						
$H_g(2)$	1 bar	343	17	372	22	405	22	383	21
	6 kbar	348	13	387	16	416	17	390	16
	47 kbar	354	7	396	15	425	15	405	14
$A_g(1)$	1 bar	493	1						
	6 kbar	496	2						
	47 kbar	514	4						
$A_g(2)$	1 bar	1447	5						
	6 kbar	1450	5						
	47 kbar	1468	6						

^a $\langle\omega_0\rangle$ and $\langle\Gamma\rangle$ refer to the weighted average values of ω_0 and Γ , respectively.

increase in pressure. The rate of increase in ω_0 for applied pressure decreases gradually above 40 kbar. The pressure coefficient $\partial\omega_0/\partial p$ is estimated to be $0.41\text{ cm}^{-1}/\text{kbar}$ ($=4.1\text{ cm}^{-1}/\text{GPa}$) for the ω_0 below 40 kbar. This value is larger than that for C_{60} , $1.1\text{ cm}^{-1}/\text{GPa}$.⁸ The Γ for the $H_g(1)$ mode increases slightly with an increase in pressure.

The ω_0 of all peaks for the $H_g(2)$ mode increase rapidly with an increase in pressure up to 30 kbar, while the ω_0 saturates above 30 kbar. The pressure dependence of the weighted average value of ω_0 is shown in Fig. 3(c). The pressure dependence is largely different from that in pristine C_{60} , in which the $H_g(2)$ mode shows the largest blueshift ($\partial\omega_0/\partial p = 2.4\text{ cm}^{-1}/\text{GPa}$) among all modes and a monotonous increase below 60 kbar.⁸ The Γ of all peaks for the $H_g(2)$ mode in Cs_3C_{60} decrease rapidly with an increase in pressure from 1 bar to 30 kbar, and shows a slight increase above 30 kbar. The pressure dependence of the weighted average value of Γ is shown in Fig. 3(d). The weighted average value of Γ also decreases rapidly up to 30 kbar and

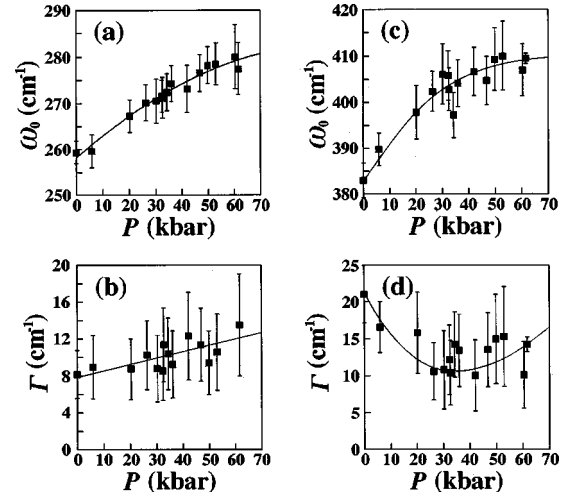


FIG. 3. Pressure dependence of (a) ω_0 and (b) Γ for $H_g(1)$ mode, and of the weighted average values of (c) ω_0 and (d) Γ in three Raman components for the $H_g(2)$ mode.

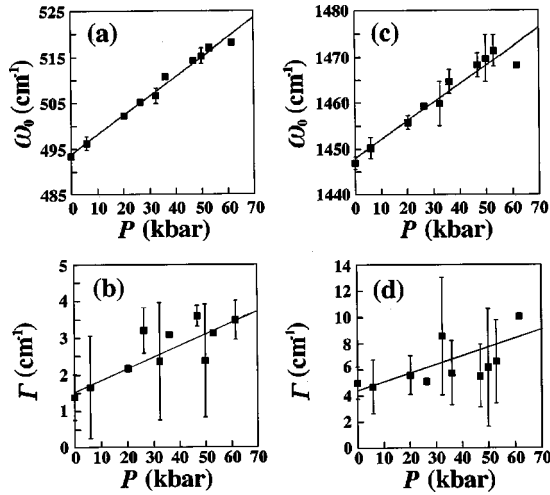


FIG. 4. Pressure dependence of (a) ω_0 and (b) Γ for the $A_g(1)$ mode, and of (c) ω_0 and (d) Γ for the $A_g(2)$ mode.

increases slightly above 30 kbar. The q values for the $H_g(1)$ and $H_g(2)$ modes are almost constant in all pressure regions.

As seen from Figs. 4(a) and 4(b), the ω_0 and Γ for the $A_g(1)$ peak increases linearly with an increase in pressure. The $\partial\omega_0/\partial p$ is estimated to be $0.42 \text{ cm}^{-1}/\text{kbar}$ ($=4.2 \text{ cm}^{-1}/\text{GPa}$), which is extremely larger than that for C_{60} ($0.94 \text{ cm}^{-1}/\text{GPa}$).⁸ The ω_0 for the $A_g(2)$ peak also increases linearly with an increase in pressure [Fig. 4(c)]. The $\partial\omega_0/\partial p$ of $0.40 \text{ cm}^{-1}/\text{kbar}$ ($=4.0 \text{ cm}^{-1}/\text{GPa}$) for the $A_g(2)$ peak is consistent with that for the $A_g(1)$ mode, and is larger than that for the $A_g(2)$ mode in C_{60} ($1.7 \text{ cm}^{-1}/\text{GPa}$).⁸ The Γ increases slightly with an increase in pressure [Fig. 4(d)]. The q values for the $A_g(1)$ and $A_g(2)$ modes are substantially constant in all pressure regions.

The mode-Grüneisen parameters $\gamma [= -(1/\kappa)(1/\omega_0)(d\omega_0/dp)]$ for the $A_g(1)$ and $A_g(2)$ modes are determined from the pressure dependence of ω_0 and the compressibility $\kappa [= (1/V)(dV/dp)]$ to be 0.28 and 9.6×10^{-2} , respectively; the κ is determined to be $3.1 \times 10^{-3} \text{ kbar}^{-1}$ for Cs_3C_{60} .⁹ The γ for the $A_g(2)$ mode is the same order as that for C_{60} (6.4×10^{-2}).¹⁰ The small γ for the $A_g(1)$ and $A_g(2)$ modes suggest that the bond lengths for the C_{60} molecule in Cs_3C_{60} are little affected by the contraction of the crystal lattice under pressure.

The contribution of the $A_g(1)$ and $A_g(2)$ modes to the λ in Cs_3C_{60} is extremely small at 1 bar in comparison with the $H_g(1)$ and $H_g(2)$ modes.⁴ These modes cannot be expected to contribute to the λ even under high pressure. Therefore, the $A_g(1)$ and $A_g(2)$ modes will be affected only by an increase in force constants of the C_{60} molecule caused by applying pressure. The intercalation of three Cs atoms into the C_{60} lattice leads to a softening of the tangential intramolecular $-C_{60}-A_g(2)$ mode by $\sim 20 \text{ cm}^{-1}$ because of a decrease in force constants of the C_{60} molecule caused by the transfer of three electrons to the antibonding LUMO orbital, i.e., charge-transfer elongation of C-C bonds.^{7,11,12} Conversely, as seen from Fig. 4(c), applying pressure of 50 kbar to Cs_3C_{60} leads to a stiffening by 20 cm^{-1} , whose variation is comparable to that caused by three-electrons transfer to a LUMO orbital in C_{60} .

The λ for Cs_3C_{60} can be estimated according to the equation,^{7,13-15}

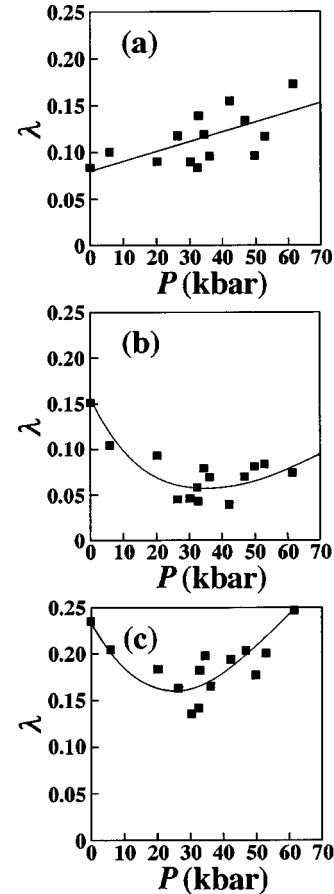


FIG. 5. Pressure dependence of λ for (a) $H_g(1)$ and (b) $H_g(2)$ modes, and of (c) total λ . The λ for the $H_g(2)$ mode was estimated from the weighted average values of ω_0 and Γ .

$$\lambda = \sum \lambda_i = \sum C \Delta \Gamma_i / [\omega_{01}^2 N(\epsilon_F)],$$

where λ_i is the λ for the i th mode. $C = d_i/\pi$, d_i being the degeneracy of the i th mode ($d = 5$ for the H_g mode, $d = 1$ for A_g mode). The $\Delta \Gamma_i$ is the difference between the Γ_i in Cs_3C_{60} and that in C_{60} ; the Γ_i at 1 bar is employed for C_{60} in all pressure regions. The $N(\epsilon_F)$ ($=9$ state $eV^{-1}C_{60}^{-1} \text{ spin}^{-1}$) (Ref. 4) determined at 1 bar is used as the $N(\epsilon_F)$ in all pressure regions. The λ for the $H_g(1)$ and $H_g(2)$ modes at 1 bar are estimated to be 0.08 and 0.15, respectively, and the total $\lambda = 0.23$, which is substantially in agreement with that reported previously.⁴ The pressure dependence of λ for the $H_g(1)$ and $H_g(2)$ modes are shown in Figs. 5(a) and 5(b); the weighted average values of the ω_0 and Γ are used in estimating the λ from the $H_g(2)$ mode. The λ for the $H_g(1)$ mode increases with an increase in pressure, while that for the $H_g(2)$ decreases rapidly from 0.15 to 0.05 up to 30 kbar and increases slightly above 30 kbar. As shown in Fig. 5(c), the total λ decreases rapidly up to 30 kbar and increases above 30 kbar. This result may be associated with the phase transition from the multiphase (bco and A15) to the single phase (bco) which is found by the pressure-dependent x-ray diffraction study.¹⁹ This suggests that a disappearance of disorder in the Cs_3C_{60} crystal plays an important role for a superconductivity.

However, the total λ estimated from the $H_g(1)$ and $H_g(2)$ modes is smaller than that (~ 0.65) expected from the Mc-Millan formula. We employed the $N(\epsilon_F)$ at 1 bar in estimat-

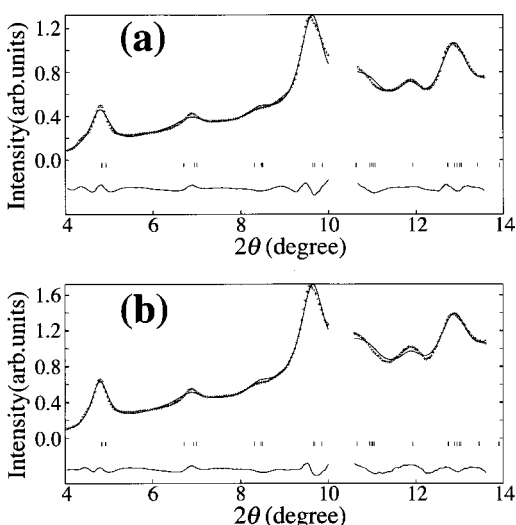


FIG. 6. X-ray diffraction patterns at (a) 101 and (b) 11 K under a pressure of 40 kbar. The crosses and solid lines refer to the experimental and the best-fitted patterns, respectively. Ticks mark the positions of allowed Bragg reflections. The difference between the experimental and the best-fitted patterns is shown by the thin lines in the bottom of each figure.

ing the λ . However, the $N(\epsilon_F)$ value should decrease with an increase in pressure according to the relation, $N(\epsilon_F) \sim t_{\text{inter}}^{-1} \sim d_{\text{inter}}^n$;^{14,15} the parameters, t_{inter} and d_{inter} , refer to the interatomic hopping integral and the interatomic distance, respectively, and the n is normally 2–3. The unit cell volume V at 30 and 60 kbar can be estimated from the pressure dependence of V for Cs_3C_{60} ⁹ to be ~ 1540 and $\sim 1410 \text{ \AA}^3$, respectively. When 3 is adopted for the n in estimating $N(\epsilon_F)$, the values of $N(\epsilon_F)$ at 30 and 60 kbar are predicted to be 90 and 85 % of that at 1 bar, respectively. When the reduction of $N(\epsilon_F)$ is taken into account, the λ at 60 kbar should increase from 0.25 to 0.3. The increase in λ is still smaller than that expected by the McMillan formula.

Figures 6(a) and 6(b) show the x-ray powder-diffraction patterns at 101 and 11 K, respectively, under a pressure of 40 kbar. Though the x-ray diffraction pattern measured at 1 bar and 295 K shows the existence of two phases of bco (95%) and A15 (5%), no A15 phase is observed for both x-ray diffraction patterns at 40 kbar shown in Figs. 6(a) and 6(b). These x-ray diffraction patterns can be indexed with a bco phase ($Immm$): $R_{wp}=3.42\%$ and $R_p=2.76\%$ at 101 K,

$R_{wp}=3.23\%$ and $R_p=2.61\%$ at 11 K. The lattice constants a , b , and c at 11 K under a pressure of 40 kbar are determined to be 11.8(1), 11.32(9), and 11.40(9) \AA respectively; the V is 1520(23) \AA^3 . The x-ray diffraction patterns suggest no structural phase transition between 11 and 101 K at 40 kbar, where the superconducting transition should occur. Therefore, it is concluded that the bco phase is the superconducting phase for Cs_3C_{60} .

¹H NMR spectrum of this sample was measured to identify a stoichiometry of NH_3 by a NMR (nuclear magnetic resonance) spectrometer (Bruker DSX400). The ¹H NMR spectrum shows that the sample contains small amounts of NH_3 ; the stoichiometry is $\text{Cs}_3\text{C}_{60}(\text{NH}_3)_{0.1}$. The V determined from the x-ray diffraction pattern at 1 bar and 295 K, 1654(4) \AA^3 , is in agreement with those reported previously for Cs_3C_{60} within the standard deviation: 1662 \AA^3 in Ref. 1 and 1659(2) \AA^3 in Ref. 2. These results suggest that the pressure-induced superconducting Cs_3C_{60} reported in Ref. 1 contains small amounts of NH_3 . The existence of NH_3 in these samples cannot be confirmed from the x-ray diffraction patterns because of extremely small amounts of NH_3 . The bco phase of Cs_3C_{60} may be stabilized by NH_3 occupying the vacancies at $4f$ and $4h$ sites where Cs atoms occupy with the occupancy of 0.75.

In conclusion, the total λ estimated from the $H_g(1)$ and $H_g(2)$ modes also shows a rapid decrease up to 30 kbar and an increase above 30 kbar. This result suggests that a disappearance of the disorder in Cs_3C_{60} crystal leads to an appearance of superconductivity. However, even under high pressure the total λ does not increase to the value (0.65) expected for Cs_3C_{60} by the McMillan formula. The small λ may show the necessity of including other H_g modes and intermolecular vibrations in estimating the e-ph coupling in Cs_3C_{60} . The x-ray diffraction patterns at 40 kbar show that the superconducting phase of Cs_3C_{60} is bco as in the case of the normal phase. Further, the ¹H NMR study suggests that the superconducting phase of Cs_3C_{60} contains small amounts of NH_3 . The origin of the pressure-induced superconductivity should further be studied.

The authors are grateful to Dr. Hiroshi Kitagawa of JAIST for his valuable suggestion in Raman measurements. The x-ray diffraction study at 40 kbar was performed under a Proposal of KEK-PF (97G201). This study was supported by a Grant-in-Aid (11165227) from the Ministry of Education, Science, Sports and Culture, Japan.

*Corresponding author. Electronic address:

kubozono@cc.okayama-u.ac.jp

¹T. T. M. Palstra *et al.*, *Solid State Commun.* **93**, 327 (1995).

²Y. Yoshida *et al.*, *Chem. Phys. Lett.* **291**, 31 (1998).

³P. Dahlke *et al.*, *J. Mater. Chem.* **8**, 1571 (1998).

⁴Y. Kubozono *et al.*, *Chem. Phys. Lett.* **298**, 335 (1998).

⁵F. Izumi, in *The Rietveld Method*, edited by R. A. Young (Oxford University, New York, 1993), p. 236.

⁶J. Winter and H. Kusmany, *Phys. Rev. B* **53**, 655 (1996).

⁷P. Zhou *et al.*, *Phys. Rev. B* **48**, 8412 (1993).

⁸D. W. Snoke *et al.*, *Phys. Rev. B* **45**, 14 419 (1992).

⁹Y. Kubozono *et al.*, in *Electronic Properties of Novel Materials—*

Science and Technology of Molecular Nanostructures, Proceedings of the XIII International Winterschool for Electronic Properties of Novel Materials, Austria, 1999, edited by H. Kuzmany *et al.*, AIP Conf. Proc. No. 486 (AIP, New York, 1999), p. 69.

¹⁰S. H. Tolbert *et al.*, *Chem. Phys. Lett.* **188**, 163 (1992).

¹¹S. J. Duclos *et al.*, *Science* **254**, 1625 (1991).

¹²K.-A. Wang *et al.*, *Phys. Rev. B* **45**, 1955 (1992).

¹³C. M. Varma *et al.*, *Science* **254**, 989 (1991).

¹⁴M. Schluter *et al.*, *Phys. Rev. Lett.* **68**, 526 (1992).

¹⁵K. Prassides *et al.*, in *Fullerene: Status and Perspectives*, edited by C. Taliani, G. Ruani, and R. Zamboni (World Scientific, Singapore, 1992), p. 147.